Springer manuscript No.
(will be inserted by the editor)

A new angle on second harmonic generation from a small hole in a metal film

Esmaeil Rahimi · **Reuven Gordon***

Received: date / Accepted: date

Abstract Bethe's theory treats a subwavelength aperture in a metal film as the combination of a parallel magnetic dipole and transverse electric dipole. For linear optics, this gives the usual dipole transmission; however, for nonlinear optics, it is interesting to consider how these two components interact. While many works have studied the nonlinear harmonic generation for metal nanoapertures, here we show that the Lorentz force dominates the second harmonic generation by an order of magnitude at angled incidence where the generation is maximized. The angular dependence matches that of the magnetic and electric dipoles accounting for Lambert's cosine law. The theoretical analysis and numerical calculations agree well with past experiments.

Keywords second harmonic generation · angle dependence · · Lorentz magnetic force · magnetic/electric dipole · Hydrodynamic theory · nonlinear scattering theory

1 Introduction

The relative importance of various hydrodynamic contributions to second harmonic generation (SHG) has been a topic of investigation for at least four decades [1]. While there is some debate about how to disentangle various contributions in practice [1, 2], theoretical works have suggested that the Lorentz contribution is negligible in common plasmonic structures [3]. Following this, we suggested that the underlying

Esmaeil Rahimi
University of Victoria, Department of Electrical and Computer Engineering, Victoria, British Columbia, V8P 5C2, Canada
E-mail: esmaeil.rahimij@gmail.com

Reuven Gordon University of Victoria, Department of Electrical and Computer Engineering, Victoria, British Columbia, V8P 5C2, Canada
Tel.: +1250-721-5179
E-mail: rgordon@uvic.ca
*corresponding author

reason why this contribution is usually weak is because it is uncommon to have both a magnetic and electric enhancement in the same location; we then went on to design a structure having simultaneous magnetic and electric resonant contributions in the same location by having two separate resonances [4]. That structure produced an unusually large second harmonic signal dominated by the Lorentz contribution. The structure, however, was quite contrived, and so it is interesting to consider if there are more natural ways to achieve an enhanced Lorentz contribution.

It is well known that subwavelength apertures in thin metal films can be treated as magnetic dipoles [5], and hence the transmission scales as the fourth power of the aperture dimension. In addition, there is an electric dipole component that arises when an out-of-plane electric field is present at the aperture [5]. This only occurs for angled incidence and so it is less commonly considered. Nevertheless, this normal contribution is important because it allows for simultaneous electric and magnetic dipoles in the same location. In this work, the cross product of these two effective dipoles is considered as a Lorentz contribution to SHG.

Fortunately, there has already been considerable research on SHG from apertures [6–38]. Of particular note are the works looking at angled contributions in ordered and disordered apertures [10, 11]. For the disordered case, it is anticipated that there is negligible contribution coming from aperture interactions and so the response is similar to a single aperture [39]. The quantitative finding of past works was that the SHG was enhanced for an angle of 50° [11]. Simulations showed that the field was highest at one edge under those conditions, which was interpreted to give the largest SHG. While this is a reasonable explanation, the relative physical origin of this SHG from the various hydrodynamic effects (separate from surface contributions) deserves further consideration.

In this work, we analyze the properties of a circular nanoaperture in a thin gold film metasurface and investigate the origin of the generated second harmonic light. The Hydrodynamic theory is used to quantitatively describe the nonlinear response. The investigated nanoaperture is identical to the past experiments [11], a 260 nm diameter aperture in a 100 nm thick gold film on quartz substrate with a 5 nm Chromium adhesion layer in between.

2 Theory of Force on Magnetic Dipole from Electric Dipole

In quasi-static regime, where the aperture size is very small compared to the wavelength ($r << \lambda$), the field transmission through a subwavelength aperture can be approximated by the radiation from the magnetic dipole $\vec{m}$ in the tangential direction and the electric dipole $\vec{p}$ in the normal direction. It is interesting to posit that the Lorentz magnetic contribution to the SHG will follow the cross product of these two dipoles.

In case of a plane wave incident at the angle θ_i with respect to the normal plane on the aperture surface, the electric dipole moment is defined as [5, 40]:

$$\vec{p} = \frac{r^3}{3\pi}\varepsilon_0 \vec{E} sin\theta_i \tag{1}$$

similarly the magnetic dipole moment can be expressed as:

$$\vec{m} = -\frac{2r^3}{3\mu_0\pi}\vec{B} \tag{2}$$

where ε_0 and μ_0 are the free space permittivity and permeability, r is the aperture radius, $\vec{E}$ and $\vec{B}$ are the incident electric field and the magnetic flux density respectively.

In case of normal incidence (θ_i=0), the radiation reduces then to that of a single magnetic radiating dipole. For transverse magnetic angled incidence, the electric dipole plays a role as well.

The equivalent $\vec{p}$ will serve as a local current and can also be expressed as:

$$\vec{p} = -i\omega\vec{J} \tag{3}$$

where $\vec{J}$ is an infinitesimal current.

The lowest order force ($\vec{F}$) on the localized current distribution in an external magnetic field exposed by the magnetic dipole component part of the nanoaperture is calculated as [41]:

$$\vec{F} = \nabla(\vec{m}\cdot\vec{B}) \tag{4}$$

This also can be found to be written as [42]:

$$\vec{F} = (\vec{m}\cdot\nabla)\vec{B} + \vec{m}\times(\nabla\times\vec{B}) \tag{5}$$

The last term in Equation 5 contains the electric dipole contribution from the Ampere-Maxwell equation [41]:

$$\nabla\times\vec{B} = \mu_0(\vec{J} - i\omega\varepsilon_0\vec{E}) \tag{6}$$

Substituting Equations 3 and 6 into Equation 5, yields:

$$\vec{F} = (\vec{m}\cdot\nabla)\vec{B} + \frac{\mu_0 i}{\omega}(\vec{m}\times\vec{p}) - i\omega\mu_0\varepsilon_0(\vec{m}\times\vec{E}) \tag{7}$$

As Equation 7 shows, a component of the force is proportional to $\vec{m}\times\vec{p}$. It is natural to consider whether the response of an aperture follows the interaction between co-located effective electric and magnetic dipoles.

3 Hydrodynamic SHG Calculation

In order to calculate the SHG, we use the hydrodynamic model of conduction electrons in the metal. The hydrodynamic model is a simple model which can address linear and nonlinear response of plasmonic metasurfaces.

In the hydrodynamic context, the Euler's momentum equation of electron gas in metal can be written as [1]:

$$\frac{\partial\vec{v}}{\partial t} + (\vec{v}\cdot\nabla)\vec{v} + \gamma\vec{v} = \frac{e}{m_e^\star}(\vec{E}(\theta) + \vec{v}\times\vec{B}(\theta)) - \frac{\beta^2}{n}\nabla n \tag{8}$$

where $\vec{v}$ and n represent the electron velocity and density, $\vec{E}(\theta)$ and $\vec{B}(\theta)$ are the local electric field and magnetic flux density due to incident electromagnetic field at θ_i, $m_e^\star$ is the electron effective mass, e is the electron charge, γ is the electron collision rate, and the last term is the quantum pressure of the electron gas due to Thomas-Fermi theory, which is neglected in the following calculations.

Expanding all the fields in Equation 8 coupled with Maxwell equations up to second order, along with the continuity equation:

$$\nabla.\vec{J} = -e\frac{\partial n}{\partial t} \tag{9}$$

The fundamental and second harmonic terms in terms of current density $\vec{J}$ can be obtained as [3]:

$$\vec{J}_1(\theta) = \frac{i}{(\omega+i\gamma)}.\frac{ne^2}{m_e^\star}\vec{E}_1(\theta) \tag{10a}$$

$$\vec{J}_2(\theta) = \frac{i}{(2\omega+i\gamma)}.\frac{ne^2}{m_e^\star}\vec{E}_2(\theta) + \vec{J}_{\mathrm{NL}}(\theta) \tag{10b}$$

The nonlinear current source, $\vec{J}_{\mathrm{NL}}(\theta)$, is given as:

$$\vec{J}_{\mathrm{NL}}(\theta) = \frac{ine^3}{m_e^{\star 2}(2\omega+i\gamma)(\omega+i\gamma)}[\vec{J}_{\mathrm{Lorentz}} + \vec{J}_{\mathrm{Coulomb}} + \vec{J}_{\mathrm{convective}}] \tag{11}$$

where

$$\begin{cases} \vec{J}_{\mathrm{Lorentz}} = -i\left(\vec{E}_1(\theta)\times\vec{B}_1(\theta)\right) \\ \vec{J}_{\mathrm{Coulomb}} = \frac{1}{\omega}\vec{E}_1(\theta)\left(\nabla\cdot\vec{E}_1(\theta)\right) \\ \vec{J}_{\mathrm{convective}} = \frac{1}{(\omega+i\gamma)}\left[\left(\nabla\cdot\vec{E}_1(\theta)\right)\vec{E}_1(\theta) + \left(\vec{E}_1(\theta)\cdot\nabla\right)\vec{E}_1(\theta)\right] \end{cases}$$

The subscripts refer to the first and the second-order fields respectively. Equation 10a gives the usual linear transmission, and equation 10b along with equation 11 give the second order response that is responsible for SHG and also rectification.

In the last set of equations as the labels show, the term $\vec{E}_1(\theta)\times\vec{B}_1(\theta)$ represents the Lorentz magnetic force contribution, the term $\vec{E}_1(\theta)(\nabla\cdot\vec{E}_1(\theta))$ represents the nonlinear Coulomb interaction and the two terms $(\nabla\cdot\vec{E}_1(\theta))\vec{E}_1(\theta) + (\vec{E}_1(\theta)\cdot\nabla)\vec{E}_1(\theta)$ indicate the contribution from electron convection.

Nonlinear scattering (NLS) theory [18,43] describes how an incident field excites local currents (through nonlinear terms described above) and these currents are coupled to a harmonic field. Here we consider an extension of this theory to angled incidence. In this case, the incident source and the scattered plane wave contain the angular dependence. So $\vec{J}_2(\theta)$ is calculated by excitation with $\vec{E}_1(\theta)$ at an angle of incidence θ_i. Then the second harmonic scattered, at angle θ_s, is calculated by reciprocity using the time reversal of a source incident at angle θ_s. θ_i and θ_s are assumed as the incident and detection angles respectively. We consider the special case of $\theta_i = \theta_s = \theta$. Our simulations found that when the incident and detection angle

matched the SHG was maximized (please see the Supporting Information) , which was also the experimental finding [11].

The SHG power, P_{SHG}, is then calculated as an overlap integral over the gold volume using the fields at fundamental frequency and second harmonic as calculated from the linear solution to Maxwell's equations:

$$P_{\mathrm{SHG}} = \int_{\mathrm{Au}} \vec{J}_{\mathrm{NL}}(\theta) \cdot \vec{E}_2(\theta) dV \tag{12}$$

Recalling Equations 10b and 11, the SHG power is then calculated as:

$$P_{\mathrm{SHG}} = \frac{ine^3}{m_e^{\star 2}(2\omega + i\gamma)(\omega + i\gamma)} [P_{\mathrm{Lorentz}} + P_{\mathrm{Coulomb}} + P_{\mathrm{convective}}] \tag{13}$$

where

$$\begin{cases} P_{\mathrm{Lorentz}} = -i \int_{\mathrm{Au}} (\vec{E}_1(\theta) \times \vec{B}_1(\theta)) \cdot \vec{E}_2(\theta) dV \\ P_{\mathrm{Coulomb}} = \frac{1}{\omega} \int_{\mathrm{Au}} \vec{E}_1(\theta) \left(\nabla \cdot \vec{E}_1(\theta) \right) \cdot \vec{E}_2(\theta) dV \\ P_{\mathrm{convective}} = \frac{1}{(\omega + i\gamma)} \int_{\mathrm{Au}} \left[\left(\nabla \cdot \vec{E}_1(\theta) \right) \vec{E}_1(\theta) + \left(\vec{E}_1(\theta) \cdot \nabla \right) \vec{E}_1(\theta) \right] \cdot \vec{E}_2(\theta) dV \end{cases}$$

In Equation 13, the terms are the Lorentz, Coulomb, and convective power contributions to the SHG.

4 FDTD Simulation of SHG

Finite-Difference Time-Domain (FDTD) simulation (Lumerical Solutions, Inc. version 8.15.736) is used to calculate the linear solutions to Maxwell's equation required for the theory of the previous section. Following the Lorentz reciprocity, which states that the scattered plane wave field leaving a structure can be modeled by the equivalent but time-reversed field incident on the structure [41]; two separate simulations are performed in this study. One at the fundamental wavelength (800 nm) which results in the electric field and magnetic flux density, $\vec{E}_1$ and $\vec{B}_1$; and one at the second harmonic wavelength (400 nm) resulting in the electric field and magnetic flux density, $\vec{E}_2$ and $\vec{B}_2$.

The metal thin film is placed in the simulation area where its surface is positioned perpendicular to the z-axis. Source waves propagating along the z-axis are generated by the Total-Field Scattered-Field (TFSF) technique [44].

The TFSF source is an advanced version of illumination by a plane wave which separates the computation region into two distinct regions: the total field region includes the sum of the incident field wave plus the scattered field and the scattered field region includes only the scattered field. TFSF source is used to prevent aperturing of the source for subwavelength simulations and to reduce interactions with the boundaries of the simulation.

The TFSF sources illuminate the structure at varying incident angles to their normal axis with the P-polarized input field. Stabilized perfectly matched layer absorbing boundary conditions are employed at all boundaries, making sure that the simulations

have no reflection at the boundaries. In the simulations, the TFSF source is used to account for the angled detection using reciprocity. This source is accurate up to large angles, and so it is not expected to be a source of error in the detection with large angles.

Only one circular aperture (unit cell) is needed in the computational area. A 1000 femtosecond simulation time has been set long enough to calculate all the existing field responses in the simulation area. The maximum mesh size was set to 5 nm covering the unit cell along x, y, and z directions. We have used the dispersion model for gold derived from the experimental data provided by Johnson and Christy [45] and CRC model for Chromium [46].

A schematic of the simulated structure along with the simulation elements is shown in Figure 1.

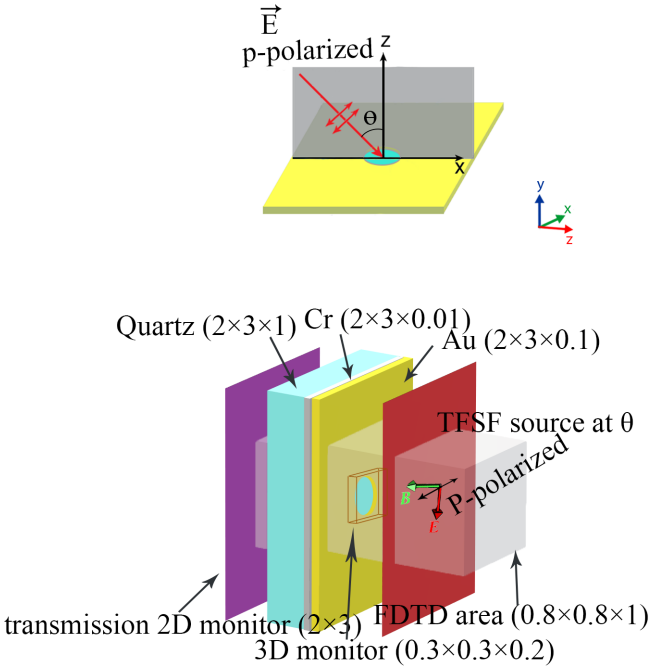

Fig. 1 A schematic of the simulated structure along with the simulation elements. Shining the P-polarized electromagnetic field at angle θ on the structure. The dimension of the elements are shown in parenthesis in microns.

First, the transmission of fundamental light at different incident angles on the metal film was simulated. A 2D power monitor positioned at the back of the aperture collects the transmitted light. Figure 2 (a) shows the simulation result for both TE and TM electromagnetic field polarization mode along with the experimental result presented in Ref [11] for comparison. A $\cos\theta$ factor is required to account for the reduced subtended area at angled detection. The FDTD simulation curve is normalized to unity power.

Second, a power monitor is set to collect the electric and magnetic fields of the fundamental and second harmonic signal at varying incident angle. A 3D index monitor also helps to identify the type of material on which the electromagnetic field is solved.

A MATLAB ©(Mathwork MATLAB ver. *R*2018*b*) script was written to calculate each SHG hydrodynamic contribution term as a function of incident angle. The total SHG was then calculated as the sum of all three contributions. Figure 2 (b) shows the result of SHG calculations along with the SHG experimental result of the past work [11]. In these simulations, the SHG power was $1.2 \times 10^{-6}\%$ of the transmitted power at the fundamental frequency for an incident field intensity of $4 \times 10^{15}\ W/m^2$.

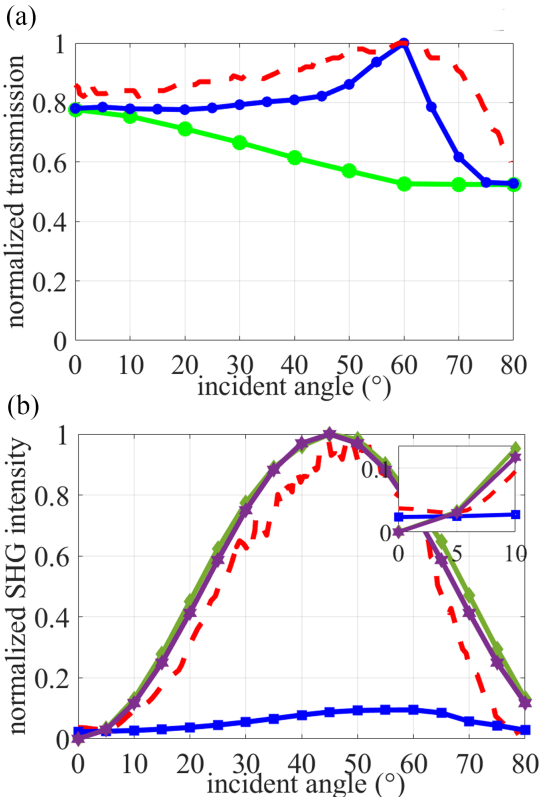

Fig. 2 a) The FDTD simulation of transmittance spectrum of the TE (green line) and TM mode of fundamental beam (red line) as a function of incidence angle, along with a digitized plot of the past experimental result of the same structure in Ref [11] (dashed red line). The curves are normalized to maximum value of experimental results. b) SHG calculation based on NLS theory as a function of incident angle for Lorentz (green line), the sum of two Coulomb and convective terms (blue line), $|\sin\theta \times \cos\theta|^2$ (purple line) along with the digitized plot of the corresponding experimental results in Ref [11] (dashed red line). The inset shows the curves plot in low angles. The curves are normalized to their maximum value of total SHG.

5 Discussion

The simulated linear transmission and NLS theory results match well with the past experiment [11]. For normal incidence, the harmonic generation has no Lorentz contribution. This is expected from Bethe's aperture theory since there is no electric dipole for normal incidence. As the incidence angle is increased, however, the Lorentz contribution becomes the dominant term and indeed the maximum of the Lorentz SHG coincides with the experimentally determined value. The Lorentz contribution is an order of magnitude larger than the other contributions at the angle of its maximum.

The angular dependence of the Lorentz contribution follows the force on a magnetic dipole from the electric dipole, considering the effective dipoles of the aperture. In particular, the magnetic dipole has no angular dependence, whereas electric dipole has a $\sin(\theta)$ dependence. The detected field should also account for Lambert's cosine law to account for the reduced subtended area with increasing angle. So overall, the cross product of these two fields will produce a detected intensity which goes as $\sin^2(\theta)\cos^2(\theta)$. This dependence is also plotted in Figure 2 (b). It is clear that this simple theoretical model agrees well with the experimental and comprehensive NLS theory results.

Due to the rotational symmetry of the structure, the SHG generated followed the incident polarization (please see the Supporting Information). The nonlinear scattering theory uses the boundary conditions of the linear solutions to Maxwell equations with nonlinear bulk source terms. A detailed analysis of the impact of these source terms in with generalized Fresnel relations is given elsewhere [47].

TE polarization was also investigated and gave reduced SHG as the angle was increased. This is expected since there is no normal electric field component for TE polarization, and so the Lorentz contribution from TM polarization is not present. Also the transverse magnetic field decreases with increasing angle and so the transmission expected from Bethe's theory is reduced. Please see the Supporting Information for the simulation results on SHG signal for TE and TM incident polarization.

6 Conclusion

In this work, we showed by comprehensive NLS theory that the SHG for a circular aperture in a metal film is dominated by the Lorentz contribution at angled incidence. The observed behavior was interpreted in terms of simple model invoking Bethe's decomposition of an aperture into its electric and magnetic field parts. Considering the force on a magnetic dipole from an electric dipole, we showed that the Lorentz contribution in this case comes from the cross product of these two dipoles.

Here we considered only the non-local and Lorentz contributions to the SHG, while others have considered as well surface contributions [15, 32, 48–55]. The Lorentz response agrees well with past experiments and so we believe that it captures the dominant physics of the nanohole configuration.

In the future, enhanced second harmonic generation from nanostructured metal films may be achieved by exploiting this angular dependence of the electric and magnetic dipoles. Here we have shown that the Lorentz contribution of the simplest cir-

cular structure is 12 times bigger than the combined convective and Coulomb contributions. It may be possible in the future to combine these enhancements with shaping of the apertures to achieve further efficiency gains.

Supporting Information

Contains more simulation results including: comparison of the calculated SHG for different incident angles of TE and TM polarization modes, calculated SHG for different incident and detection angle and, the detected SHG for different polarization angle.

Funding

This research was supported by the NSERC CREATE, Materials for Enhanced Energy Technologies (MEET) program, and an NSERC Discovery Grant.

Conflict of interest

The authors declare that they have no conflict of interest.

References

1. JE Sipe, VCY So, M Fukui, and GI Stegeman. Analysis of second-harmonic generation at metal surfaces. *Physical Review B*, 21(10):4389, 1980.
2. Fu Xiang Wang, Francisco J Rodríguez, Willem M Albers, Risto Ahorinta, JE Sipe, and Martti Kauranen. Surface and bulk contributions to the second-order nonlinear optical response of a gold film. *Physical Review B*, 80(23):233402, 2009.
3. Cristian Ciracì, Ekaterina Poutrina, Michael Scalora, and David R Smith. Origin of second-harmonic generation enhancement in optical split-ring resonators. *Physical Review B*, 85(20):201403, 2012.
4. Esmaeil Rahimi, Haitian Xu, Byoung-Chul Choi, and Reuven Gordon. Lorentz nanoplasmonics for nonlinear generation. *Nano Letters*, 18(12):8030–8034, 2018.
5. Hans Albrecht Bethe. Theory of diffraction by small holes. *Physical Review*, 66(7-8):163, 1944.
6. A Lesuffleur, LKS Kumar, and R Gordon. Apex-enhanced second-harmonic generation by using double-hole arrays in a gold film. *Physical Review B*, 75(4):045423, 2007.
7. Antoine Lesuffleur, L Kiran Swaroop Kumar, and Reuven Gordon. Enhanced second harmonic generation from nanoscale double-hole arrays in a gold film. *Applied Physics Letters*, 88(26):261104, 2006.
8. Ghazal Hajisalem, Aftab Ahmed, Yuanjie Pang, and Reuven Gordon. Plasmon hybridization for enhanced nonlinear optical response. *Optics Express*, 20(28):29923–29930, 2012.
9. Fatemeh Eftekhari and Reuven Gordon. Enhanced second harmonic generation from noncentrosymmetric nanohole arrays in a gold film. *IEEE Journal of Selected Topics in Quantum Electronics*, 14(6):1552–1558, 2008.
10. Marc Airola, Yongdong Liu, and Steve Blair. Second-harmonic generation from an array of subwavelength metal apertures. *Journal of Optics A: Pure and Applied Optics*, 7(2):S118, 2005.
11. T Xu, X Jiao, GP Zhang, and S Blair. Second-harmonic emission from sub-wavelength apertures: Effects of aperture symmetry and lattice arrangement. *Optics Express*, 15(21):13894–13906, 2007.
12. JAH Van Nieuwstadt, M Sandtke, RH Harmsen, Franciscus B Segerink, JC Prangsma, Stefan Enoch, and L Kuipers. Strong modification of the nonlinear optical response of metallic subwavelength hole arrays. *Physical Review Letters*, 97(14):146102, 2006.

13. Peter Schön, Nicolas Bonod, Eloïse Devaux, Jérôme Wenger, Hervé Rigneault, Thomas W Ebbesen, and Sophie Brasselet. Enhanced second-harmonic generation from individual metallic nanoapertures. *Optics Letters*, 35(23):4063–4065, 2010.
14. Tiberiu-Dan Onuta, Matthias Waegele, Christopher C DuFort, William L Schaich, and Bogdan Dragnea. Optical field enhancement at cusps between adjacent nanoapertures. *Nano Letters*, 7(3):557–564, 2007.
15. M Scalora, MA Vincenti, D De Ceglia, V Roppo, M Centini, N Akozbek, and MJ Bloemer. Second- and third-harmonic generation in metal-based structures. *Physical Review A*, 82(4):043828, 2010.
16. Hua Lu, Xueming Liu, Renlong Zhou, Yongkang Gong, and Dong Mao. Second-harmonic generation from metal-film nanohole arrays. *Applied Optics*, 49(12):2347–2351, 2010.
17. Kitsakorn Locharoenrat. Second harmonic generation based on strong field enhancement in metallic nanostructured surface. *Materials Science*, 20(4):387–391, 2014.
18. Kevin O'Brien, Haim Suchowski, Junsuk Rho, Alessandro Salandrino, Boubacar Kante, Xiaobo Yin, and Xiang Zhang. Predicting nonlinear properties of metamaterials from the linear response. *Nature Materials*, 14(4):379–383, 2015.
19. Jongwon Lee, Nishant Nookala, J Sebastian Gomez-Diaz, Mykhailo Tymchenko, Frederic Demmerle, Gerhard Boehm, Markus-Christian Amann, Andrea Alù, and Mikhail A Belkin. Ultrathin second-harmonic metasurfaces with record-high nonlinear optical response. *Advanced Optical Materials*, 4(5):664–670, 2016.
20. Fu Xiang Wang, Francisco J Rodriguez, Hannu Husu, and Martti Kauranen. Second-order nonlinear optical properties of metal nanostructures and metamaterials. *Nonlinear Opt. Quantum Opt*, 40:43–56, 2010.
21. Christos Argyropoulos, Giuseppe D'Aguanno, and Andrea Alu. Giant second-harmonic generation efficiency and ideal phase matching with a double ε-near-zero cross-slit metamaterial. *Physical Review B*, 89(23):235401, 2014.
22. K Liu, L Zhan, ZY Fan, MY Quan, SY Luo, and YX Xia. Enhancement of second-harmonic generation with phase-matching on periodic sub-wavelength structured metal film. *Optics Communications*, 276(1):8–13, 2007.
23. Brian K Canfield, Sami Kujala, Konstantins Jefimovs, Yuri Svirko, Jari Turunen, and Martti Kauranen. A macroscopic formalism to describe the second-order nonlinear optical response of nanostructures. *Journal of Optics A: Pure and Applied Optics*, 8(4):S278, 2006.
24. EH Barakat, M-P Bernal, and FI Baida. Second harmonic generation enhancement by use of annular aperture arrays embedded into silver and filled by lithium niobate. *Optics Express*, 18(7):6530–6536, 2010.
25. Ben-Li Wang, Rui Wang, RJ Liu, XH Lu, Jimin Zhao, and Zhi-Yuan Li. Origin of shape resonance in second-harmonic generation from metallic nanohole arrays. *Scientific Reports*, 3(1):1–8, 2013.
26. Wenjun Fan, Shuang Zhang, KJ Malloy, SRJ Brueck, NC Panoiu, and RM Osgood. Second harmonic generation from patterned gaas inside a subwavelength metallic hole array. *Optics Express*, 14(21):9570–9575, 2006.
27. Wenjun Fan, Shuang Zhang, N-C Panoiu, A Abdenour, S Krishna, RM Osgood, KJ Malloy, and SRJ Brueck. Second harmonic generation from a nanopatterned isotropic nonlinear material. *Nano Letters*, 6(5):1027–1030, 2006.
28. Ajay Nahata, Richard A Linke, T Ishi, and K Ohashi. Enhanced nonlinear optical conversion from a periodically nanostructured metal film. *Optics Letters*, 28(6):423–425, 2003.
29. Adi Salomon, Marcin Zielinski, Radoslaw Kolkowski, Joseph Zyss, and Yehiam Prior. Size and shape resonances in second harmonic generation from silver nanocavities. *The Journal of Physical Chemistry C*, 117(43):22377–22382, 2013.
30. Nikifor Rakov, Francisco E Ramos, and Mufei Xiao. Strong second-harmonic radiation from a thin silver film with randomly distributed small holes. *Journal of Physics: Condensed Matter*, 15(23):L349, 2003.
31. MA Vincenti, D De Ceglia, Vito Roppo, and M Scalora. Harmonic generation in metallic, gaas-filled nanocavities in the enhanced transmission regime at visible and uv wavelengths. *Optics Express*, 19(3):2064–2078, 2011.
32. Jérémy Butet, Benjamin Gallinet, Krishnan Thyagarajan, and Olivier JF Martin. Second-harmonic generation from periodic arrays of arbitrary shape plasmonic nanostructures: a surface integral approach. *JOSA B*, 30(11):2970–2979, 2013.
33. Ming Kang, Yongnan Li, Kai Lou, Si-Min Li, Qiang Bai, Jing Chen, and Hui-Tian Wang. Second-harmonic generation in one-dimensional metal gratings with dual extraordinary transmissions. *Journal of Applied Physics*, 107(5):053108, 2010.

34. Maria Antonietta Vincenti, Vincenzo Petruzzelli, Antonella D'Orazio, Francesco Prudenzano, Mark J Bloemer, Neset Aközbek, and Michael Scalora. Second harmonic generation from nanoslits in metal substrates: applications to palladium-based h2 sensor. *Journal of Nanophotonics*, 2(1):021851, 2008.
35. Renlong Zhou, Hua Lu, Xueming Liu, Yongkang Gong, and Dong Mao. Second-harmonic generation from a periodic array of noncentrosymmetric nanoholes. *JOSA B*, 27(11):2405–2409, 2010.
36. Michele Celebrano, Margherita Zavelani-Rossi, Dario Polli, G Cerullo, Paolo Biagioni, Marco Finazzi, Lamberto Duo, M Labardi, Maria Allegrini, J Grand, et al. Mapping local field enhancements at nanostructured metal surfaces by second-harmonic generation induced in the near field. *Journal of Microscopy*, 229(2):233–239, 2008.
37. Sinjeung Park, Jae W Hahn, and Jae Yong Lee. Doubly resonant metallic nanostructure for high conversion efficiency of second harmonic generation. *Optics Express*, 20(5):4856–4870, 2012.
38. Elena Drobnyh and Maxim Sukharev. Plasmon enhanced second harmonic generation by periodic arrays of triangular nanoholes coupled to quantum emitters. *The Journal of Chemical Physics*, 152(9):094706, 2020.
39. MC Hughes and R Gordon. Optical transmission properties and enhanced loss for randomly positioned apertures in a metal film. *Applied Physics B*, 87(2):239–242, 2007.
40. Christoffel Jacob Bouwkamp. Diffraction theory. *Reports on progress in physics*, 17(1):35, 1954.
41. John David Jackson. *Classical electrodynamics*. John Wiley & Sons, 2007.
42. Timothy H Boyer. The force on a magnetic dipole. *American Journal of Physics*, 56(8):688–692, 1988.
43. Yong Zeng, Walter Hoyer, Jinjie Liu, Stephan W Koch, and Jerome V Moloney. Classical theory for second-harmonic generation from metallic nanoparticles. *Physical Review B*, 79(23):235109, 2009.
44. Allen Taflove and Susan C Hagness. *Computational electrodynamics: the finite-difference time-domain method*. Artech House, 2005.
45. Peter B Johnson and R-WJPrB Christy. Optical constants of the noble metals. *Physical Review B*, 6(12):4370, 1972.
46. William M Haynes. *CRC handbook of chemistry and physics*. CRC press, 2014.
47. Nicolaas Bloembergen and PS Pershan. Light waves at the boundary of nonlinear media. *Physical review*, 128(2):606, 1962.
48. Carlo Forestiere, Antonio Capretti, and Giovanni Miano. Surface integral method for second harmonic generation in metal nanoparticles including both local-surface and nonlocal-bulk sources. *JOSA B*, 30(9):2355–2364, 2013.
49. Jérémy Butet and Olivier JF Martin. Evaluation of the nonlinear response of plasmonic metasurfaces: Miller's rule, nonlinear effective susceptibility method, and full-wave computation. *JOSA B*, 33(2):A8–A15, 2016.
50. NC Panoiu, WEI Sha, DY Lei, and GC Li. Nonlinear optics in plasmonic nanostructures. *Journal of Optics*, 20(8):083001, 2018.
51. P Guyot-Sionnest and YR Shen. Local and nonlocal surface nonlinearities for surface optical second-harmonic generation. *Physical Review B*, 35(9):4420, 1987.
52. TF Heinz. Nonlinear surface electromagnetic phenomena. *by H.-E. Ponath and GI Stegeman (Elsevier Science Publishers BV, Amsterdam, 1991) p*, 353, 1991.
53. P Guyot-Sionnest, W Chen, and YR Shen. General considerations on optical second-harmonic generation from surfaces and interfaces. *Physical Review B*, 33(12):8254, 1986.
54. M Corvi and WL Schaich. Hydrodynamic-model calculation of second-harmonic generation at a metal surface. *Physical Review B*, 33(6):3688, 1986.
55. Daniel Timbrell, Jian Wei You, Yuri S Kivshar, and Nicolae C Panoiu. A comparative analysis of surface and bulk contributions to second-harmonic generation in centrosymmetric nanoparticles. *Scientific Reports*, 8(1):1–9, 2018.